Journal of Photochemistry and Photobiology A: Chemistry 201 (2009) 111–120

Contents lists available at ScienceDirect

Journal of Photochemistry and Photobiology A: Chemistry

journal homepage: www.elsevier.com/locate/jphotochem

Nanosized cadmium sulfide in polyelectrolyte protected mesoporous sphere: A stable and regeneratable photocatalyst for visible-light-induced removal of organic pollutants

You-Hao Yang, Nan Ren, Ya-Hong Zhang, Yi Tang*

Department of Chemistry, Shanghai Key Laboratory of Molecular Catalysis and Innovative Materials and Laboratory of Advanced Materials, Fudan University, Shanghai 200433, People's Republic of China

ARTICLE INFO

Article history:
Received 5 January 2008
Received in revised form 28 July 2008
Accepted 8 October 2008
Available online 5 November 2008

Keywords:
Visible-light-induced photocatalysis
Degradation of organic compound
Cadmium sulfide
Mesoporous silica sphere
Photocorrosion

ABSTRACT

An unusually stable and regeneratable nanosized CdS-based catalyst for visible-light-induced photocatalysis was developed by combining the protection effect of polyelectrolyte and the spatial confinement of mesopores. This catalyst was fabricated by coating a layer of poly(diallyl dimethylammonium) chloride (PDDA) around nanosized CdS pre-incorporated hexagonal mesoporous silica (HMS) sphere, and named as CdS/HMS–PDDA. In contrast to the catalyst without PDDA-coating (CdS/HMS), which loses its activity at 3rd run, CdS/HMS–PDDA can completely degrade the organic pollutants for over 22 runs. Noticeably, CdS/HMS–PDDA can be facilely regenerated by H_2S treatment, and the catalyst shows the same capability as the fresh one even after 6 regenerations (accumulatively 151 runs). No cadmium leakage is detected from CdS/HMS–PDDA during the photocatalytic processes, promising its environmental compatibility. A series of characterization experiments reveal that the polyelectrolyte layer effectively prevents the cadmium species from leakage, and further delays the photocorrosion of CdS via a back reaction occurred by use of photogenerated electrons remaining in CdS, endowing the catalyst with high stability and regeneratability.

1. Introduction

Nowadays, environmental pollution caused by organic compounds has far-reaching negative consequences in the lives of human being. Hazardous organic pollutants such as dyes and phenolic compounds emitted from various sources have caused severe ecological problems due to their nondegradability and toxicity. Therefore, the removal of these toxicants in water has become one of the most important issues in environmental science [1–4]. Heterogeneous photocatalysis is believed to be a proper method for the decontamination and mineralization of organic pollutants because of its high efficiency, low energy consumption and satisfactory environmental compatibility [5].

Various catalysts have already been employed in photocatalysis [1–9]. Among them, semiconductors are the most widely used photocatalysts [4,9]. Generally, the band gap excitation of the semiconductor leads to the formation of electron–hole pairs (e^-–h^+ pairs) that can generate free radical species with superior redox ability and drive photocatalytic processes. Among the various semiconductors, TiO_2 is the most extensively investigated catalyst owing to its advantages such as high activity, excellent chemical stability, low toxicity and low cost [10–13]. However, TiO_2 can only be effectively activated by ultra-violet (UV) light and thereby, its response to solar light is rather poor because of the low proportion of UV light (about 5% [4]). Although some colored contaminants such as dyes can be self-sensitizedly degraded by TiO_2 under visible light [4,14,15], such photocatalytic process would cease once the chromophores of dyes are destroyed. To harvest visible light with TiO_2, modification methods such as dye-sensitization [4,16,17], doping [18–20], ion-implanting [21,22] and heterojunction [23] are necessary in order to extend its absorption band into visible range [24], however concerns still exist regarding the stability of the modifier and the efficiency of the electron transfer between the modifier and TiO_2 [25].

Another way to realize efficient photocatalysis under visible light irradiation involves the application of the semiconductors with relatively narrow band gap [26]. For instance, CdS and some other chalcogenide semiconductors [27,28] have shown great prospect in visible-light-induced photocatalysis. With a proper band gap (2.4 eV) and an appropriate absolute redox potential, CdS acquires good response to the solar spectrum and exhibits significant photophysicochemical properties for water-splitting [29,30],

* Corresponding author at: Department of Chemistry, Fudan University, 220 Handan Road, Shanghai 200433, People's Republic of China. Tel.: +86 21 55664125; fax: +86 21 65641740.
E-mail address: yitang@fudan.edu.cn (Y. Tang).

1010-6030/$ – see front matter © 2008 Elsevier B.V. All rights reserved.
doi:10.1016/j.jphotochem.2008.10.012

solar cells [31], photocatalytic synthesis [32] as well as for the photocatalytic removal of organic pollutants [1,33–35]. However, CdS is prone to react with the photogenerated holes and then undergo photocorrosion under light irradiation [36], resulting in a poor chemical stability during photocatalytic processes. Furthermore, the cadmium species generated by photocorrosion will escape into the liquid phase, leading to a secondary pollution by heavy metal. The photocorrosion together with the consequent leakage of cadmium species has become the biggest obstacle for the practical application of CdS-based catalyst in water treatment [35]. In past decades, tremendous efforts have been devoted to the enhancement of its activity and the improvement of its photostability. The former can be achieved by the utilization of CdS nanoparticle. Due to the size quantization effect, the nanosizing of CdS particle not only increases the band gap but also decreases the possibility of the e^-–h^+ recombination [37,38], and consequently promotes the photocatalytic activity of CdS [39]. The latter, as the essential key for practical photocatalytic application of CdS, mainly involves the immobilization of CdS onto proper supports such as layered compounds [40], Nafion [41], Al_2O_3 [42,43], zeolite [44] and mesoporous materials [45,46]. However, the photostability of the reported CdS catalysts is far from the desired level, and CdS catalyst with superior photostability and less cadmium leakage is still being pursued.

Herein, a stable and regeneratable CdS photocatalyst was fabricated via *in situ* generation of CdS nanoparticles in hexagonal mesoporous silica (HMS) sphere followed by coating a polyelectrolyte layer outside. The catalyst not only shows high efficiency in photocatalytic removal of organic pollutants, but also exhibits long lifetime and resistance against cadmium leakage under light irradiation. Importantly, the catalyst can be completely regenerated through H_2S treatment, and there is no decay on its photocatalytic performance even after six regenerations (corresponding to 600 h of irradiation). These distinguished features are attributed to the anti-leakage and the photocorrosion-delaying effects of the polyelectrolyte layer on the basis of the results of various characterization methods including X-ray diffraction (XRD), UV–visible, Raman and atomic absorption spectroscopy (AAS).

2. Experimental

2.1. Materials

The poly(diallyl dimethylammonium) chloride (PDDA, M_w = 200,000) was purchased from Aldrich. The commercial TiO_2 catalyst (Degussa P25, specific surface area 50 m^2/g) was supplied from Degussa. The dyes including Eosin B, Methylene Blue, Neutral Red and Sudan I were obtained from Shanghai Chemical Reagent Company. Phenol, *p*-chlorophenol and *p*-nitrophenol were purchased from Runjie Chemical Reagent Company. Hydroquinone was obtained from Lingfeng Chemical Reagent Company. 2,4,6-trichlorophenol was purchased from Arcos. All chemicals were used as received without further purification.

2.2. Fabrication of catalysts

HMS spheres were synthesized according to the previously reported method [47], followed by calcination at 600 °C for 6 h to remove the surfactant in the mesopores. The introduction of cadmium species into HMS was conducted using the method we previously reported [48]. To achieve complete conversion of the incorporated cadmium into CdS, the prepared composite was subsequently sulfurized by treating it in H_2S atmosphere. In detail, the sulfurization was carried out in an air-isolated vessel. A stream of H_2S was produced by dropping HCl into Na_2S and filled into the vessel, and then the vessel was heated to and kept at 100 °C for 2 h. To obtain the final catalyst, the sulfurized sample was ultrasonically dispersed in 0.2 wt% aqueous solution of PDDA with a liquid/solid ratio of 10:1 (ml/g), and then placed at ambient temperature for 2 h. After washing with water and centrifugation, the final catalyst with polyelectrolyte protective layer was obtained and named as CdS/HMS–PDDA.

For comparison, a catalyst without polyelectrolyte protective layer (named as CdS/HMS) was also prepared in the same way as described above but omitting the step of PDDA-coating, and a sample without CdS was obtained directly by coating PDDA onto HMS and was named as HMS–PDDA.

2.3. Irradiated reactions

The photocatalytic reactor was a quartz vessel with an internal equipped xenon lamp (120 W, $\lambda > 420$ nm) surrounded by a quartz jacket with a water-cooling system. In a typical photocatalytic reaction, 20 mg of catalyst was suspended in 80 ml of aqueous solution of dye or phenol at certain concentration, and the temperature in the reactor was maintained at 30 °C. Before photocatalytic experiment, the suspension was stirred in dark for 10 min to exclude the possible influence of reactant adsorption on the determination of the photocatalytic activity. Afterwards, the suspension was exposed to the irradiation of xenon lamp for photocatalysis. Airflow was continuously pumped into the system during the whole process. The photodegradation of the organic reactants was monitored by UV–visible absorption spectroscopy. At specified time intervals, 1 ml of the reaction suspension was taken from the reactor and centrifuged to separate the catalyst. The separated catalyst was then returned to the reactor to avoid the loss of catalyst during sampling. The content of the reactants in the supernate was determined at their specified detection wavelength, in detail, 506 nm for Eosin B, 665 nm for Methylene Blue, 522 nm for Neutral Red, 478 nm for Sudan I, 270 nm for phenol, 280 nm for *p*-chlorophenol, 298 nm for hydroquinone, 278 nm for *p*-nitrophenol and 311 nm for 2,4,6-trichlorophenol. After each photocatalytic run, the catalyst was separated from the suspension by centrifugation for the next run, while the supernate was collected for further analysis such as cadmium content and mineralization degree of organic pollutants. The former was determined by employing AAS while the latter was measured by total organic carbon (TOC) value and chemical oxygen demand (COD) value. The COD value was determined by the amount of potassium dichromate ($K_2Cr_2O_7$) reduced by the sample after 2 h of refluxing in a medium of sulfuric acid and silver sulfate catalyst. The detection limit of this method is 1 mg/l.

In order to estimate the photocorrosion of the catalysts under irradiation, the catalysts after sulfurized in moist H_2S stream were irradiated under the open-air condition at ambient temperature. Typically, 100 mg of catalyst was tiled carefully to form a thin wafer (diameter = 4 cm) on an agate mortar in a box shielding from other light sources, and a xenon lamp (120 W, $\lambda > 420$ nm) was hung 5 cm above the mortar. The photocorrosion degree of the catalysts was characterized by XRD, Raman spectroscopy and UV–visible diffuse reflectance absorption spectroscopy.

2.4. Regeneration of catalysts

The regeneration of catalysts was carried out by a re-sulfurization process on the spent catalyst powder. In detail, the spent catalyst was placed in an air-isolated vessel. A stream of H_2S was produced by dropping HCl into Na_2S and filled into the vessel. Then the vessel was placed thermostatically at 100 °C for 2 h. The effluent gas was absorbed by saturated Na_2SO_3 solution. Precau-

tions should be carefully taken to avoid the H_2S leakage and isolate the system from air.

2.5. Characterization of catalysts and reactions

Scanning electron microscopy (SEM) measurements were performed by a Philips XL30 D6716 instrument at an operating voltage of 25 kV, while transmission electron microscopy (TEM) experiments with selected area electron diffraction (SAED) were carried out with a JEOL JEM-2010 instrument at an operating voltage of 200 kV. The XRD patterns were recorded on a Rigaku D/Max-rB 12KW diffractometer (Cu Kα). The mean crystallite diameter of CdS nanoparticles was calculated by Scherrer formula. X-ray fluorescence (XRF) experiments were performed by a BRUKER-AXS S4 Explorer apparatus. AAS analysis was performed by a Hitachi Z-5000 Polarized Zeeman Atomic Absorption Spectrometer with the detection limit of 0.002 mg/l. Infrared (IR) spectra were obtained by a Nicolet FT-IR 360 spectrometer while Raman spectra were recorded by a LabRam-1B spectrometer. Adsorption/desorption isotherms of nitrogen were recorded with a Micromeritics ASAP 2000 instrument at 77 K. The UV–visible spectroscopic experiments were carried out with a Shimadzu UV 2450 spectrophotometer. During measurement, the liquid samples were placed in quartz cuvettes with 1 cm of path length. The diffuse reflectance UV–visible spectra were obtained with an ISR-2200 attachment. The TOC value was determined on a Shimadzu TOC-VCPN Analyzer with the detection limit of 0.05 mg/l.

3. Results

3.1. Characterization of catalysts

Fig. 1a and 1b respectively depicts the SEM and TEM images of the original HMS spheres before the introduction of CdS, which clearly exhibit a uniform spherical morphology with the average diameter of about 1.2 μm. The XRD (Fig. 2A-a and 2B-a) and SAED patterns (Fig. 1c) prove their mesoporous structure with amorphous wall. The N_2 adsorption/desorption experiment (Fig. 3) further confirms their mesoporosity with the Brunauer–Emmett–Teller (BET) specific surface area of 643 m^2/g and the most probable pore diameter of 2.6 nm. These results are all in agreement with the literature [47]. The unique three-dimensional interconnected mesoporous structure of HMS would act as an excellent nanoreactor for CdS nanoparticle formation and photocatalytic reactions, while the micrometric size of HMS spheres ensures considerable convenience for the manipulation in practice.

After incorporating CdS and coating PDDA, the final catalyst CdS/HMS–PDDA (Fig. 1d) well retains the spherical morphology of original HMS. The TEM image (Fig. 1e) presents a large number of black dots within the HMS sphere, indicating that CdS nanoparticles have been generated in the mesopores of HMS. The contents of Cd and S in the CdS/HMS–PDDA are determined by XRF to be 5.82 and 2.16 wt% respectively, and the molar ratio of Cd:S is about 3:4. The SAED pattern (Fig. 1f) displays clear diffraction rings with discontinuous diffraction spots. These diffraction rings can be indexed to (0 0 2), (1 1 0), (1 1 2) planes of CdS referred to its XRD result (cf. Fig. 2B-b).

The XRD pattern of CdS/HMS–PDDA is depicted in Fig. 2. The small-angle XRD pattern of CdS/HMS–PDDA (Fig. 2A-b) shows almost the same diffraction peak as that of original HMS (Fig. 2A-a), demonstrating the preservation of mesoscopic structure in CdS/HMS–PDDA. The tiny shift of the diffraction peak to a smaller angle suggests the slight enlargement of the mesopores as the result of the formation of cadmium sulfide nanoparticles. Meanwhile, the wide-angle XRD pattern of CdS/HMS–PDDA (Fig. 2B-b) presents the diffraction peaks of CdS crystal, which have been indexed to (0 0 2), (1 1 0), (1 1 2) planes of the hexagonal greenockite phase (space group: $P6_3/mmc$) (JCPDS 41-1049) in good accordance with the SAED pattern (Fig. 1f). The mean crystallite size of CdS nanoparticles

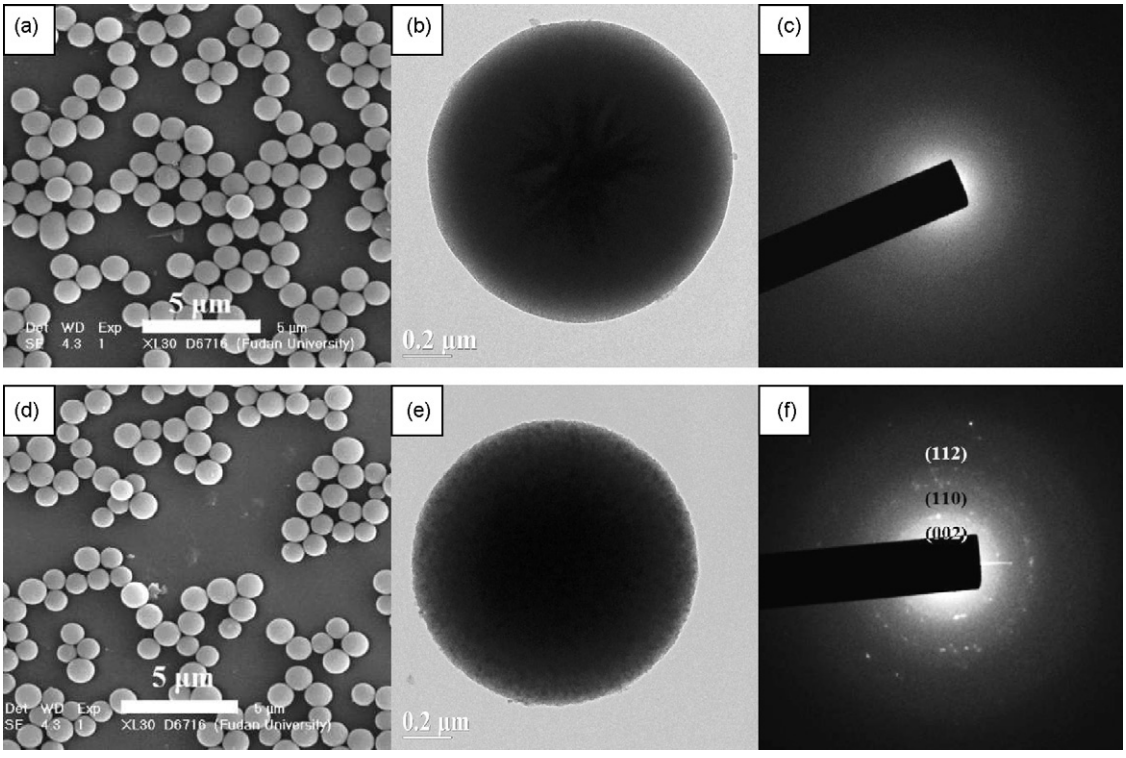

Fig. 1. SEM image (a), TEM image (b) and SAED pattern (c) of HMS; and SEM image (d), TEM image (e) and SAED pattern (f) of CdS/HMS–PDDA.

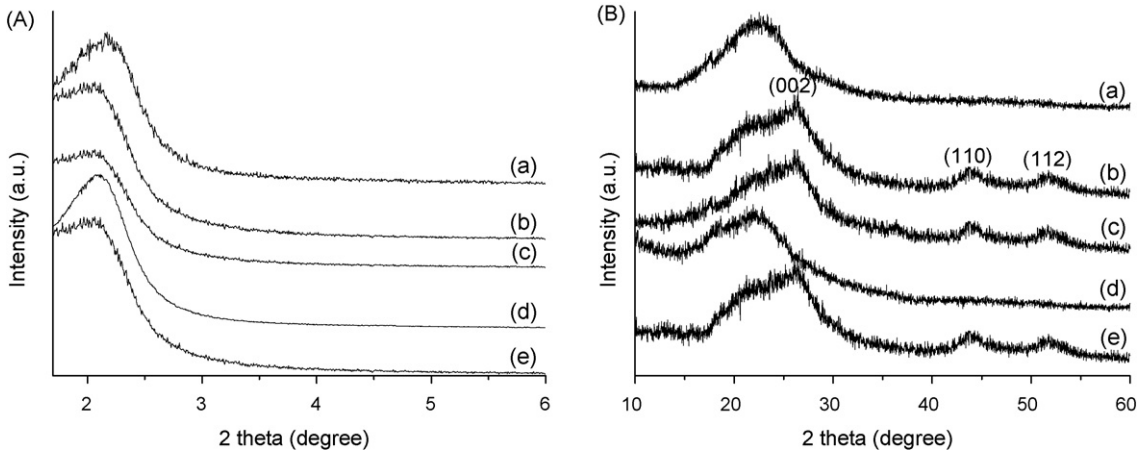

Fig. 2. The small-angle (A) and wide-angle (B) XRD patterns of HMS (a), the fresh CdS/HMS–PDDA (b) and that after irradiation for 100 h (c) and 150 h (d), and the sample regenerated by H_2S gas treatment (e).

is 2.6 nm estimated by Scherrer formula using the (1 1 0) reflection at 43.7° (2θ). This value is in good agreement with the most probable pore diameter of HMS, indicating that the mesopore of HMS acts as a spatially confined nanoreactor for the growth of cadmium sulfide particles. A similar effect has also been reported by Xu et al. [45] on the fabrication of CdS nanoparticles in MCM-41 and SBA-15. The quantum-sized CdS [37] generated in mesopore is supposed to have stronger redox ability and better surface electron transfer than the bulky CdS [38], promising higher activity for the photocatalytic degradation of organic pollutants. Besides, the spatial-confinement-effect outlined by Shchukin and Sviridov [49] and the interaction between CdS and silica reported by Kisch et al. [50,51] are also suggested to be helpful for the photocatalytic activity of CdS/HMS–PDDA.

Fig. 3 shows the nitrogen adsorption/desorption isotherms and the corresponding Barrett–Joyner–Halenda (BJH) pore diameter distribution of CdS/HMS and CdS/HMS–PDDA. After the *in situ* incorporation of CdS nanoparticles, the mesoporous structure of HMS is well retained, while the BET specific surface area drops from 643 m^2/g of HMS to 583 m^2/g of CdS/HMS, illustrating that the generated CdS nanoparticles occupy a part of the mesopores in HMS. Interestingly, after the coating of PDDA, the peak of the mesopores of original HMS disappears in the pore diameter distribution curve (Fig. 3) although the XRD pattern of CdS/HMS–PDDA (Fig. 2A-b) still

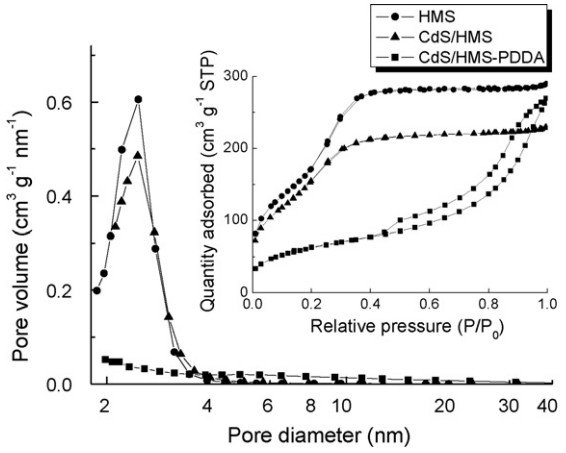

Fig. 3. N_2 adsorption/desorption isotherm of HMS, CdS/HMS and CdS/HMS–PDDA (inset); and their BJH pore diameter distributions calculated according to the corresponding adsorption isotherms.

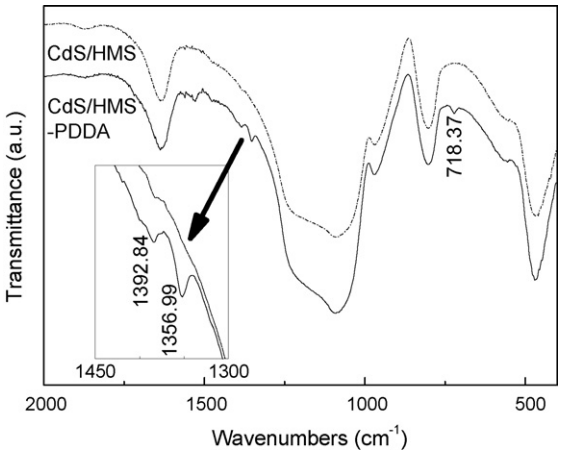

Fig. 4. IR spectra of CdS/HMS and CdS/HMS–PDDA. The inset is the magnified spectra between 1450 and 1300 cm^{-1}.

shows the existence of the mesostructure. This phenomenon can be explained by that the PDDA shell has been well coated onto the catalyst, and under the condition of the nitrogen adsorption experiment (dry state), the PDDA is in unswelled (or shrunk) form which inhibits the entrance of nitrogen molecules into the mesopores.

IR was also adopted to prove the existence of PDDA on the final catalyst and the result is shown in Fig. 4. CdS/HMS–PDDA clearly exhibits the absorption bands at 1393, 1357 and 718 cm^{-1} besides those belonging to CdS/HMS. The band at 718 cm^{-1} is assigned to the C–H in-plane bending vibrational mode of methylene in PDDA and the other two are related to the C–H stretching vibrational mode of methyl in PDDA [52].

According to the above results, the structure of the CdS/HMS–PDDA can be illustrated by Scheme 1. HMS sphere

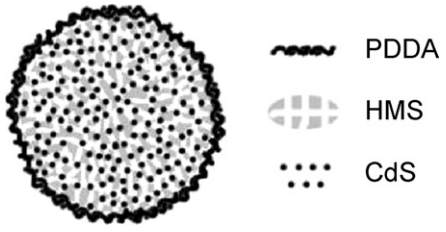

Scheme 1. The illustrated scheme of the structure of CdS/HMS–PDDA.

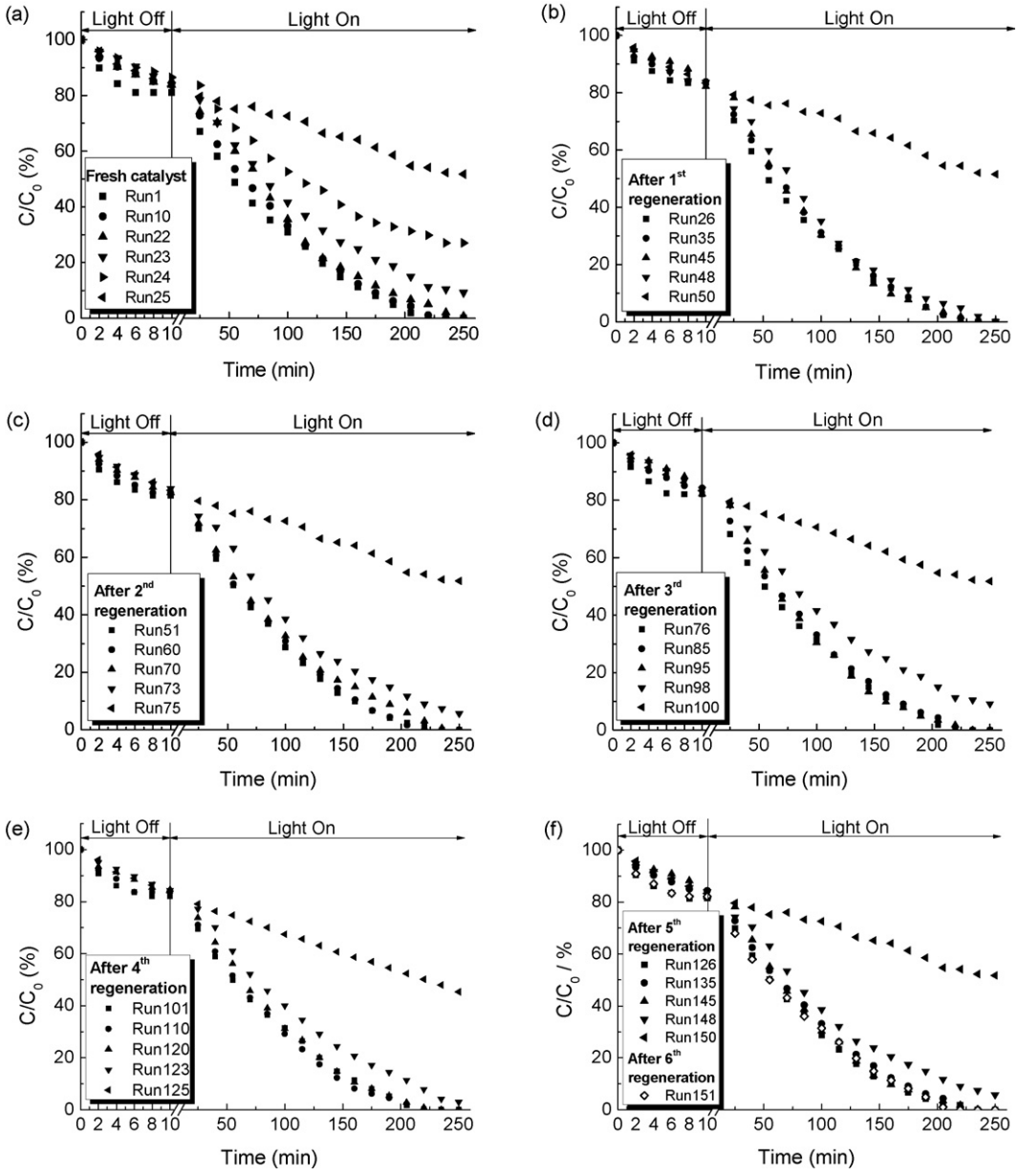

Fig. 5. Results of the visible-light-induced degradation of Eosin B on fresh CdS/HMS–PDDA (a) and on the sample after 1st–6th regeneration (b–f).

acts as the support for the CdS nanoparticles, which promises the size of CdS in nanoscale due to the spatial confinement of mesopores in HMS. The PDDA exists as a protective shell around the CdS-pretrapped HMS sphere, forming a catalyst with capsular structure. Such structure would benefit the photocatalytic reactions as proved by the following catalytic experiments.

3.2. Catalytic test

3.2.1. Degradation of dyes

Eosin B is a widely used stain with xanthene structure and is harmful if swallowed, inhaled or absorbed through skin. Considering its resistance to self-photolysis and biodegradation [53], the photocatalytic degradation of Eosin B is of importance. Fig. 5 shows the photocatalytic degradation of Eosin B on CdS/HMS–PDDA under the irradiation of xenon lamp, and the initial concentration of Eosin B solution is 1×10^{-4} M. For comparison, CdS/HMS, HMS–PDDA and a commercial TiO_2 (Degussa P25) have also been tested under the same reaction conditions (Fig. 6).

It can be observed from Figs. 5 and 6 that a dramatic improvement has been achieved on the photocatalytic stability by coating the layer of PDDA on catalyst. The CdS/HMS–PDDA is able to completely degrade Eosin B for 22 runs and is still partially active at 25th run (Fig. 5a), while the catalyst without PDDA-coating (CdS/HMS) completely loses its activity at 3rd run (Fig. 6c). Noticeably, CdS/HMS–PDDA can be regenerated by a re-sulfurization process. After being treated in H_2S atmosphere at 100 °C for 2 h, the deactivated catalyst totally restores its activity to the same level as that of the fresh one (Run 26 in Fig. 5b), and is again able to photodegrade Eosin B for over 22 runs (Fig. 5b). This cycle of the photocatalysis–regeneration can be repeated for several times (Fig. 5c–f). Even after 6 regenerations, both the activity and the reusability of CdS/HMS–PDDA remain unchanged (cf. 151st run, ◊ in Fig. 5f). This result implies that the photocatalytic degradation and the regeneration processes can be further continued.

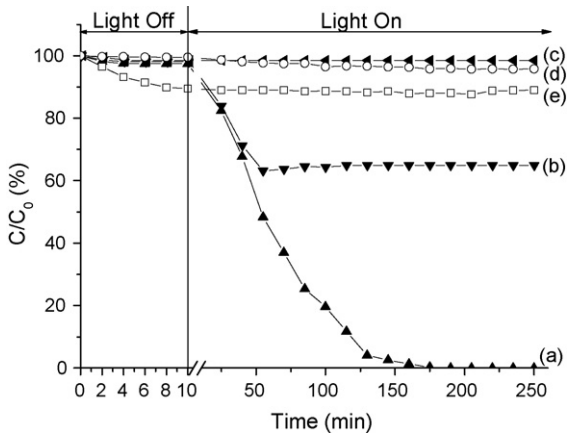

Fig. 6. Results of the visible-light-induced degradation of Eosin B on CdS/HMS in 1st (a), 2nd (b) and 3rd run (c); and the visible-light-induced degradation of Eosin B on P25 (d) and HMS–PDDA (e).

To further describe the effectiveness of CdS/HMS–PDDA on the photocatalytic degradation of Eosin B under visible light, the Degussa P25 TiO_2 and HMS–PDDA have also been tested under the same condition. No appreciable degradation takes place on Degussa P25 (Fig. 6d), indicating that neither band-gap-excited degradation nor sensitized degradation process occurs under visible light. In the case of the HMS–PDDA, no degradation of Eosin B takes place except for a small concentration decrease during the initial 10 min in dark (Fig. 6e), illustrating that the sample without CdS acts only as an adsorbent. The adsorption of Eosin B molecules on the PDDA-coated samples can be explained by the electrostatic attraction between the cationic polyelectrolyte PDDA and the Eosin B with negative charges in aqueous solution (which can be proved by the results shown in Fig. 7, where the cationic dye Methylene Blue shows no adsorption on PDDA). The influence of adsorption on the determination of photocatalytic activity would be excluded by adopting a pre-adsorption process before lighting.

Photocorrosion and the consequent cadmium leakage are considered as the fatal problems of CdS in photocatalysis. To investigate the possible cadmium leakage of CdS/HMS–PDDA during the photocatalysis, cadmium contents in the supernate after photocatalytic reactions have been measured by AAS (Table 1). It can be clearly observed that the leakage of cadmium has been effectively avoided on CdS/HMS–PDDA. Except for the tiny amount of cadmium detected in the solution during the initial three runs (probably due to the existence of small quantity of cadmium outside the PDDA layer), the cadmium concentration in the supernate is always below the detection limit of AAS (0.002 mg/l), which fully complies with the norms of various nations and organizations on drinking water quality in force, e.g. 3 μg/l of World Health Organization (Guidelines for Drinking-water Quality, 3rd ed., Vol. 1, Geneva, 2004), 5 μg/l of European Union (Drinking Water Standards, Council Directive 98/83/EC on the quality of water intended for human consumption, Adopted by the Council on 3 November 1998), 5 μg/l of U.S.A. (2004 Edition of the Drinking Water Standards and Health Advisories, Winter 2004, USEPA) and 5 μg/l of People's Republic of China (Ministry of Health P.R. China, GB 5749-2006, Standards for Drinking Water Quality, 2006). This result clears out the threat of heavy metal pollution for CdS/HMS–PDDA. Table 1 also summarizes the mineralization degree of Eosin B after the photocatalytic degradation on CdS/HMS–PDDA. Both TOC and COD values show that the mineralization degree of Eosin B reaches over 95%, indi-

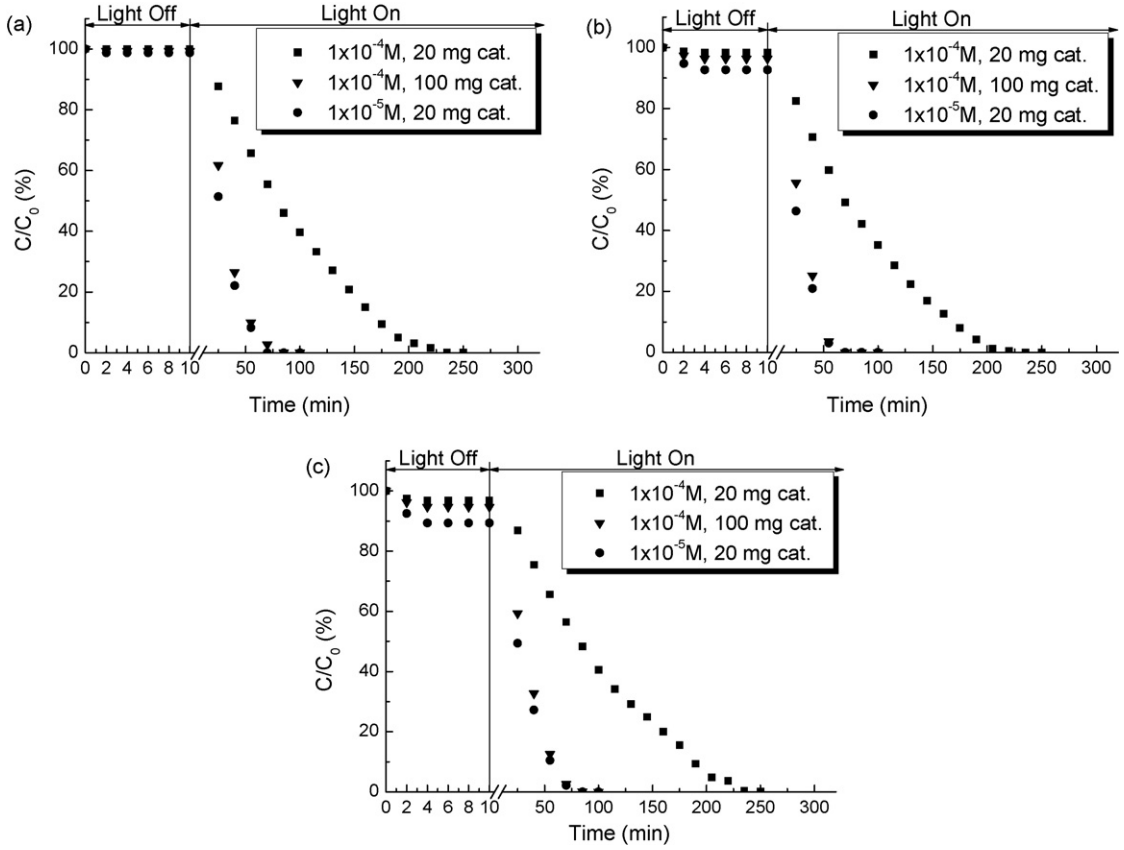

Fig. 7. Results of the visible-light-induced degradation of Methylene Blue (a), Neutral Red (b) and Sudan I (c) on CdS/HMS–PDDA at different initial dye concentrations and different catalyst amounts.

Table 1
Cadmium leakage and mineralization in the photocatalytic degradation of Eosin B.

Sample	Leakage		Mineralization[a]					
	Run	Cd (mg/l)	Run	TOC[b] (mg/l)	$(TOC_0 - TOC)/TOC_0$ (%)	Run	COD[b] (mg/l)	$(COD_0 - COD)/COD_0$ (%)
CdS/HMS–PDDA								
Before regeneration	1	0.057	1	0.6	99	1	n.d.[c]	~100
	2	0.040	10	1.0	98	4	n.d.	~100
	3	0.026	14	0.9	98	8	n.d.	~100
	5	0.002	18	0.8	98	12	n.d.	~100
	9	n.d.[c]	21	1.4	97	20	n.d.	~100
	13	n.d.	–	–	–	–	–	–
	19	0.002	–	–	–	–	–	–
	25	n.d.	–	–	–	–	–	–
After 1st regeneration	26	n.d.	26	0.7	98	30	n.d.	~100
	28	n.d.	40	0.9	98	44	n.d.	~100
	34	n.d.	45	1.1	97	–	–	–
	46	n.d.	47	1.6	96	–	–	–
	50	n.d.	–	–	–	–	–	–
After 2nd regeneration	51	n.d.	52	0.6	99	60	n.d.	~100
	70	n.d.	72	1.7	96	–	–	–
	75	n.d.	–	–	–	–	–	–
After 3rd regeneration	76	n.d.	77	1.1	97	85	n.d.	~100
	95	n.d.	97	1.0	98	–	–	–
	100	n.d.	–	–	–	–	–	–
After 4th regeneration	101	n.d.	102	0.9	98	110	n.d.	~100
	120	n.d.	121	1.6	96	–	–	–
	125	n.d.	–	–	–	–	–	–
After 5th regeneration	126	n.d.	127	1.1	97	135	n.d.	~100
	145	n.d.	147	1.9	96	146	n.d.	~100
	150	n.d.	–	–	–	–	–	–
CdS/HMS								
	1	3.1	–	–	–	–	–	–
	2	2.1	–	–	–	–	–	–

[a] TOC_0 = 42.6 mg/l, COD_0 = 40 mg/l. All samples were diluted to 250 ml.
[b] Measured after the absorbance at detection wavelength reaches 0, meaning that the dye molecules are completely degraded.
[c] n.d. = not detected.

cating that organic carbon can be effectively converted into CO_2 on this catalyst.

Besides Eosin B, stubborn dyes such as Methylene Blue, Neutral Red and Sudan I are also widely used in industry and are harmful to living things. The photocatalytic degradation of these dyes at initial concentrations of 1×10^{-4} and 1×10^{-5} M is also evaluated on CdS/HMS–PDDA under visible light. The results are shown in Fig. 7. Similar to the Eosin B, all these dyes can be completely degraded within 240 min when 20 mg of catalyst is put into 80 ml of the dye solutions at initial concentration of 1×10^{-4} M. In the cases of lower dye concentration (e.g. 1×10^{-5} M) or higher catalyst amount (e.g. 100 mg in 80 ml of solution), the degradation would finish within only 60 min. According to the mineralization data summarized in Table 2, over 92% of the organic carbon of these three dyes has been mineralized after photocatalytic degradation.

3.2.2. Degradation of phenolic compounds

Phenol and its derivatives are common industrial pollutants and their removal is important in wastewater treatment. However, they are not able to sensitize the catalysts under visible light because they themselves have no chromophore for absorbing visible light. Therefore, the research on the photocatalytic removal under visible light would be significant for phenolic compounds. Fig. 8a displays the UV–visible absorption spectra of *p*-chlorophenol during the photocatalytic degradation on CdS/HMS–PDDA under visible light. It is found that the absorption bands related to the aromatic structure of *p*-chlorophenol fades away with the increasing of reaction time and totally disappears after 3 h. Fig. 8b shows the photocatalytic activity of CdS/HMS–PDDA in the degradation of phenol, *p*-chlorophenol, *p*-nitrophenol, 2,4,6-trichlorophenol and hydroquinone (all with the initial concentration of 1×10^{-4} M). All

Table 2
Mineralization of various dyes at different concentration on CdS/HMS–PDDA under visible light irradiation.

Dye	Initial concentration (M)	TOC			COD		
		TOC_0 (mg/l)	TOC[a] (mg/l)	$(TOC_0 - TOC)/TOC_0$ (%)	COD_0 (mg/l)	COD[a] (mg/l)	$(COD_0 - COD)/COD_0$ (%)
Methylene Blue	1×10^{-4}	28.2	1.4	95	108	n.d.[b]	~100
	1×10^{-5}	2.9	n.d.[b]	~100	11	n.d.	~100
Neutral Red	1×10^{-4}	26.6	2.1	92	97	n.d.	~100
	1×10^{-5}	2.7	n.d.	~100	10	n.d.	~100
Sudan I	1×10^{-4}	36.4	2.9	92	122	n.d.	~100
	1×10^{-5}	3.7	n.d.	~100	13	n.d.	~100

[a] Measured after the absorbance at detection wavelength reaches 0, meaning that the dye molecules are completely degraded.
[b] n.d. = not detected.

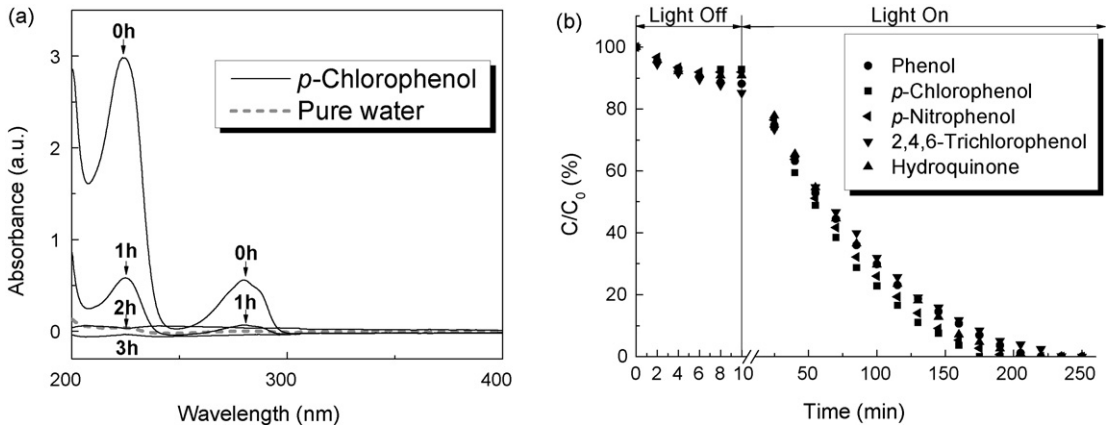

Fig. 8. UV–visible absorption spectra of pure water and *p*-chlorophenol solution irradiated for 0, 1, 2 and 3 h (a); and results of the visible-light-induced degradation of phenol, *p*-chlorophenol, *p*-nitrophenol, 2,4,6-trichlorophenol and hydroquinone using CdS/HMS–PDDA (b).

Table 3
Mineralization of phenolic compounds on CdS/HMS–PDDA under visible light irradiation.

Sample	TOC			COD		
	TOC_0 (mg/l)	TOC[a] (mg/l)	$(TOC_0 - TOC)/TOC_0$ (%)	COD_0 (mg/l)	COD[a] (mg/l)	$(COD_0 - COD)/COD_0$ (%)
p-Chlorophenol	41.1	1.1	97	32	n.d.[b]	~100
Phenol	40.3	1.1	97	25	n.d.	~100
2,4,6-Trichlorophenol	42.0	1.5	96	52	n.d.	~100
p-Nitrophenol	31.6	1.8	94	20	n.d.	~100
Hydroquinone	38.0	3.0	92	37	n.d.	~100

[a] Measured after the absorbance at detection wavelength reaches 0, meaning that the phenolic compounds are completely degraded.
[b] n.d. = not detected.

of these compounds could be completely degraded within 240 min. The TOC and COD data listed in Table 3 declare the efficient mineralization of these phenolic compounds. These facts indicate that the efficient degradation and mineralization of phenol and its derivatives can be implemented under visible light over CdS/HMS–PDDA catalyst.

4. Discussion

All the above results on the photocatalytic degradation of both dyes and phenolic compounds indicate that CdS/HMS–PDDA is an efficient catalyst for the degradation and mineralization of organic compounds under visible light. Its excellent photostability promises that its activity not only can last for about 25 runs (corresponding to an irradiated time of 100 h) but also can be completely recovered by H_2S treatment. More than 150 runs (corresponding to an irradiated time of 600 h accumulatively) have been reached for the photocatalytic degradation of organic compounds with six times of regeneration, and this photocatalytic application and regeneration processes could be further continued. However, without PDDA-coating, CdS/HMS totally loses its activity at 3rd run, which heavily hampers the practical application of CdS in photocatalysis as reported in previous literature [35].

To understand the reason why CdS/HMS–PDDA has a far superior stability than the catalyst without PDDA-coating (CdS/HMS), the cadmium contents in the fresh and the spent catalysts as well as the cadmium leakage during photocatalytic reactions are compared with each other. The data of cadmium concentration in the supernate collected after photocatalytic reactions have been listed in Table 1, and Table 4 lists the data of cadmium content in the catalyst powders after the specified photocatalytic runs. It can be clearly observed that, without the presence of PDDA-coating, CdS/HMS suffers a severe leakage of cadmium. Almost all cadmium has escaped from the catalyst after two runs (Table 1), and in parallel, no cadmium could be detected in the CdS/HMS powder after three runs (Table 4). This result can be used to explain the phenomenon shown in Fig. 6, in which CdS/HMS shows no activity at 3rd run. Since the irreversible damage caused by the cadmium leakage has occurred on the catalyst, the loss of its activity cannot be retrieved. On the contrary, the catalyst with PDDA-coating (CdS/HMS–PDDA) is able to effectively resist the cadmium leakage. No cadmium leakage can be detected after three runs (Table 1). Correspondingly, except for the slight decrease of cadmium content (from 5.8 to 5.4 wt%) in the initial three runs (Table 4), the pre-incorporated cadmium is well retained. Even after 151 runs, the cadmium content in the catalyst powder still remains at 5.2 wt%, indicating that the PDDA layer does prevent the leakage of cadmium and thus provides the premise for the regeneration of catalyst. It has been reported that [54], in the presence of oxygen, the cadmium species caused by CdS photocorrosion are mainly Cd^{2+} and $Cd^{2+}S^{-}$. The prevention of PDDA on the Cd leakage could be explained by its electrostatic repulsion and/or mechanical obstruction towards these cationic cadmium species.

On the other hand, it is believed that the photocorrosion is the ultimate reason for the loss of photoactivity and the concomitant cadmium leakage. Therefore, to delay the photocorrosion would be

Table 4
Cadmium contents of fresh and used CdS/HMS–PDDA and CdS/HMS.

Sample	Cd content (wt %)	
	CdS/HMS–PDDA	CdS/HMS
Fresh	5.8	5.8
After 3rd run	5.4	Not detected
After 25th run	5.4	–
After 50th run	5.3	–
After 151st run	5.2	–

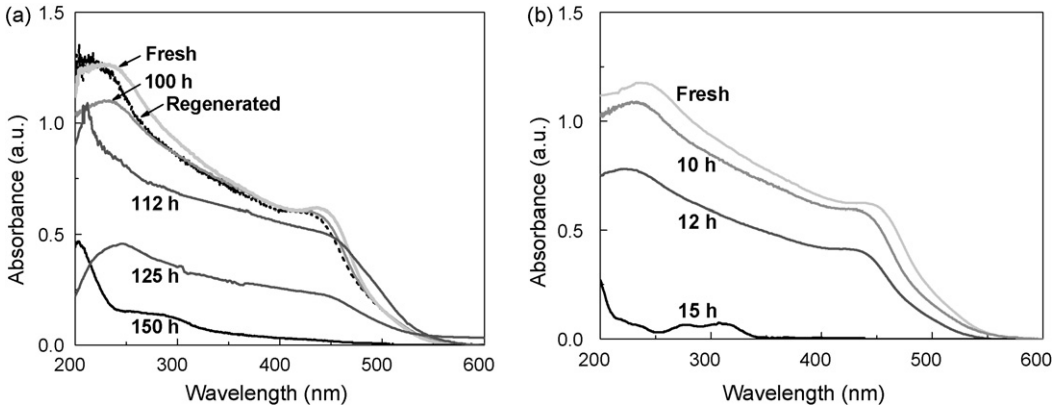

Fig. 9. The diffuse reflectance UV–visible absorption spectra of CdS/HMS–PDDA (a) and CdS/HMS (b) irradiated under visible light.

the key for prolonging the lifetime of CdS-based photocatalysts. To investigate the cause for the delay of photocorrosion on the PDDA-coated catalyst, CdS/HMS–PDDA and CdS/HMS have been irradiated under visible light in open-air condition. Under this condition, the leakage of cadmium species that would happen in aqueous solution does not exist so that the photocorrosion process can be solely estimated. As shown in Fig. 9, the fresh samples of both CdS/HMS–PDDA and CdS/HMS clearly exhibit the 1s–1s absorption of CdS [55,56] at 445 nm. This band promises the efficient utilization of solar energy as it covers the main peak of the solar spectrum of sunlight reaching the earth's atmosphere (around 460 nm) [18]. Under light irradiation, the CdS/HMS without PDDA-coating suffers severe corrosion. CdS/HMS partly loses its visible light absorption after 12 h of irradiation, and no longer has response to visible light after 15 h of irradiation, indicating the CdS has been destroyed by the photocorrosion. In comparison with CdS/HMS, CdS/HMS–PDDA retains its photoactivity for much longer time. The 1s–1s absorption band of CdS remains without obvious change even after 100 h and this band can still be observed after 125 h, approximately 10 times as the case of CdS/HMS. Moreover, as shown by the dot curve in Fig. 9a, the visible absorption band of the photocorroded catalyst can be recovered to the same level as that of the fresh sample by H_2S treatment. This result can well explain the recovery of the photocatalytic activity of the catalyst after regeneration (Fig. 5).

According to the reports of Henglein [54,57], the CdS photocorrosion in the presence of oxygen follows the mechanism below:

$$CdS(s) + h\nu \rightarrow CdS(e^- + h^+) \quad (1)$$

$$e^- + O_2 \rightarrow O_2^- \quad (2)$$

$$h^+ + CdS(s) \rightarrow Cd^{2+}S^- \quad (3)$$

$$Cd^{2+}S^- + O_2^- + O_2 \rightarrow Cd^{2+} + SO_4^{2-} \quad (4)$$

As described above, the cationic cadmium species generated from the photocorrosion can be well held in the mesoporous silica sphere covered by cationic PDDA layer, and the arrested cationic $Cd^{2+}S^-$ species can probably undergo a back reaction with photogenerated electrons on CdS surface [58] as Eq. (5),

$$e^- + Cd^{2+}S^- \rightarrow CdS \quad (5)$$

which significantly reduces the apparent photocorrosion rate of CdS. Although the photocorrosion of CdS could not be totally compensated through Eq. (5), the deactivated CdS/HMS–PDDA can still be regenerated through the reaction between H_2S and the cationic cadmium species held in the catalyst.

Analogously, the same trend of the deactivation and regeneration of CdS/HMS–PDDA can also be observed from XRD patterns (Fig. 2). After 100 h of irradiation, the diffraction peaks of CdS remains without obvious change (Fig. 2B-c). These peaks disappeared after 150 h of irradiation (Fig. 2B-d), indicating that the photocorrosion has caused the destruction of CdS nanoparticles. Fortunately, after the regeneration process, the catalyst exhibits the XRD pattern (Fig. 2B-e) similar to that of the fresh one (Fig. 2B-b), declaring that CdS in the catalyst has been recovered. Due to the spatial confinement of mesopores, the size of the regenerated CdS is almost the same as that of the fresh catalyst determined from the diffraction peak width. To confirm the regeneratability of the CdS/HMS–PDDA in practical photocatalytic process, we also investigated the Raman spectra of the fresh catalyst, the catalyst after degrading Eosin B for 25 runs (the deactivated catalyst) and the regenerated one (Fig. 10). The fresh catalyst exhibits absorption bands at 231 and 300 cm^{-1}, which can be attributed to *E1* transverse of CdS [59]. These absorption bands related to CdS disappear after 25 runs and can be completely recovered after H_2S treatment.

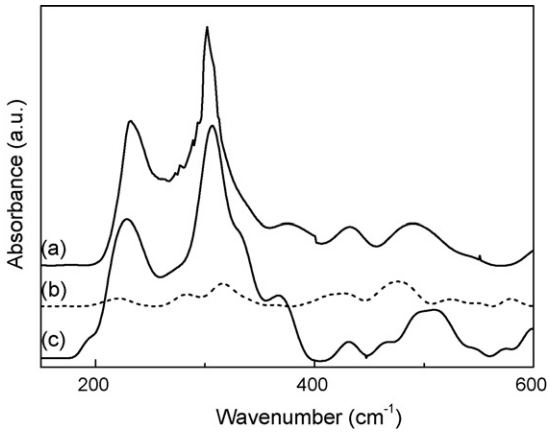

Fig. 10. Raman spectra of the fresh CdS/HMS–PDDA (a), the sample used after 25 runs (b) and the sample regenerated by H_2S treatment (c).

5. Conclusion

Utilizing the protective effect of polyelectrolyte layer as well as the spatial confinement of mesopores, an unusually stable and regeneratable catalyst CdS/HMS–PDDA for visible-light-induced photocatalysis has been fabricated. In contrast to the catalyst without protective PDDA layer (CdS/HMS), which lost its activity at 3rd run, CdS/HMS–PDDA achieved complete degradation and efficient mineralization of organic compounds for more than 22 photocatalytic runs (correspondingly over 80 h) before regeneration. The

PDDA-coating catalyst can be facilely regenerated by H_2S treatment, promising its extraordinary reusability. Accumulatively 151 runs (correspondingly 600 h) of photocatalytic degradation have been achieved so far through six times of regeneration, and more cycles of photocatalysis–regeneration are being further continued in our laboratory. Importantly, no cadmium leakage from CdS/HMS–PDDA can be detected during the photocatalysis except for the initial three runs, promising the catalyst to be environmentally compatible. The PDDA layer coated over the catalyst acts as the key factor for the stability and regeneratability of CdS/HMS–PDDA. It significantly enhances the photostability of CdS under irradiation by delaying its photocorrosion and efficiently prevents the leakage of cadmium species from the catalyst into liquid phase, promising the regeneration of the catalyst by H_2S treatment. With the integration of these intriguing advantages, CdS/HMS–PDDA could be an ideal catalyst for visible-light-induced photocatalysis.

Acknowledgments

This work was supported by the Major State Basic Research Development Program (2003CB615807), the NSFC (30828010, 20803010 and 20721063) and the STCSM (075211013, 08251203000 and 06DJ14006). The authors thank Dr. A.G. Dong of Washington University in St. Louis for the help in refining the language.

References

[1] A.P. Davis, C.P. Huang, Water Res. 24 (1990) 543–550.
[2] M.R. Hoffmann, S.T. Martin, W. Choi, D.W. Bahnemann, Chem. Rev. 95 (1995) 69–96.
[3] D.S. Bhatkhande, V.G. Pangarkar, A.A.C.M. Beenackers, J. Chem. Technol. Biotechnol. 77 (2001) 102–116.
[4] D. Chatterjee, J. Photochem. Photobiol. C 6 (2005) 186–205.
[5] J.W. Tang, Z.G. Zou, J.H. Ye, Angew. Chem. Int. Ed. 43 (2004) 4463–4466.
[6] S. Rodrigues, K.T. Ranjit, S. Uma, I.N. Martyanov, K.J. Klabunde, J. Catal. 230 (2005) 158–165.
[7] S. Rodrigues, S. Uma, I.N. Martyanov, K.J. Klabunde, J. Catal. 233 (2005) 405–410.
[8] J. Wang, S. Uma, K.J. Klabunde, Micropor. Mesopor. Mater. 75 (2004) 143–147.
[9] K. Rajeshwar, N.R. de Tacconi, C.R. Chenthamarakshan, Chem. Mater. 13 (2001) 2765–2782.
[10] A. Wold, Chem. Mater. 5 (1993) 280–283.
[11] A.L. Linsebigler, G.Q. Li, J.T. Yates Jr., Chem. Rev. 95 (1995) 735–758.
[12] A. Fujishima, T.N. Rao, D.A. Tryk, J. Photochem. Photobiol. C 1 (2000) 1–21.
[13] J.M. Macák, M. Zlámal, J. Krýsa, P. Schmuki, Small 3 (2007) 300–304.
[14] M. Stylidi, D.I. Kondarides, X.E. Verykios, Appl. Catal. B 47 (2004) 189–201.
[15] J.C. Zhao, C.C. Chen, W.H. Ma, Top. Catal. 35 (2005) 269–278.
[16] V. Iliev, J. Photochem. Photobiol. A 151 (2002) 195–199.
[17] D. Chatterjee, A. Mahata, J. Photochem. Photobiol. A 165 (2004) 19–23.
[18] R. Asahi, T. Morikawa, T. Ohwaki, K. Aoki, Y. Taga, Science 293 (2001) 269–271.
[19] S.U.M. Khan, M. Al-Shahry, W.B. Ingler Jr., Science 297 (2002) 2243–2245.
[20] S. Sakthivel, H. Kisch, Angew. Chem. Int. Ed. 42 (2003) 4908–4911.
[21] A. Zecchina, C. Lamberti, J. Am. Chem. Soc. 129 (2007) 2822–2828.
[22] M. Anpo, M. Takeuchi, J. Catal. 216 (2003) 505–516.
[23] J.E. Evans, K.W. Springer, J.Z. Zhang, J. Chem. Phys. 101 (1994) 6222–6225.
[24] H. Kisch, L. Zang, C. Lange, W.F. Maier, C. Antonius, D. Meissner, Angew. Chem. Int. Ed. 37 (1998) 3034–3036.
[25] H.G. Kim, D.W. Hwang, J.S. Lee, J. Am. Chem. Soc. 126 (2004) 8912–8913.
[26] C. Lettmann, H. Hinrichs, W.F. Maier, Angew. Chem. Int. Ed. 40 (2001) 3160–3164.
[27] J.S. Hu, L.L. Ren, Y.G. Guo, H.P. Liang, A.M. Cao, L.J. Wan, C.L. Bai, Angew. Chem. Int. Ed. 44 (2005) 1269–1273.
[28] N.F. Zheng, X.H. Bu, H. Vu, P.Y. Feng, Angew. Chem. Int. Ed. 44 (2005) 5299–5303.
[29] W.F. Shangguan, A. Yoshida, J. Phys. Chem. B 106 (2002) 12227–12230.
[30] D.W. Jing, L.J. Guo, J. Phys. Chem. B 110 (2006) 11139–11145.
[31] Y. Kang, D. Kim, Sol. Energy Mater. Sol. C 90 (2006) 166–174.
[32] H. Kisch, W. Lindner, Chem. Unserer Zeit. 35 (2001) 250–257.
[33] Y. Ku, C.-B. Hsieh, Ind. Eng. Chem. Res. 31 (1992) 1823–1826.
[34] H.M. Yang, C.H. Huang, X.W. Li, R.R. Shi, K. Zhang, Mater. Chem. Phys. 90 (2005) 155–158.
[35] W.Z. Tang, C.P. Huang, Chemosphere 30 (1995) 1385–1399.
[36] N. Kakuta, J.M. White, A. Campion, A.J. Bard, M.A. Fox, S.E. Webber, J. Phys. Chem. 89 (1985) 48–52.
[37] Y. Nosaka, J. Phys. Chem. 95 (1991) 5054–5058.
[38] A. Hagfeldt, M. Grätzel, Chem. Rev. 95 (1995) 49–68.
[39] B. Pal, T. Torimoto, K. Okazaki, B. Ohtani, Chem. Commun. (2007) 483–485.
[40] Y. Guo, H. Zhang, Y. Wang, Z.L. Liao, G.D. Li, J.S. Chen, J. Phys. Chem. B 109 (2005) 21602–21607.
[41] S.M. Wang, P. Liu, X.X. Wang, X.Z. Fu, Langmuir 21 (2005) 11969–11973.
[42] M.K. Arora, A.S.K. Sinha, S.N. Upadhyay, Ind. Eng. Chem. Res. 37 (1998) 1310–1316.
[43] T. Hirai, Y. Bando, I. Komasawa, J. Phys. Chem. B 106 (2002) 8967–8970.
[44] M. Sathish, B. Viswanathan, R.P. Viswanath, Int. J. Hydrogen Energy 31 (2006) 891–898.
[45] W. Xu, Y.T. Liao, D.L. Akins, J. Phys. Chem. B 106 (2002) 11127–11131.
[46] G.Q. Guan, T. Kida, K. Kusakabe, K. Kimura, E. Abe, A. Yoshida, Appl. Catal. A 295 (2005) 71–78.
[47] M. Grün, C. Büchel, D. Kumar, K. Schumacher, B. Bidlingmaier, K.K. Unger, Stud. Surf. Sci. Catal. 128 (2000) 155–165.
[48] N. Ren, B. Wang, Y.H. Yang, Y.H. Zhang, W.L. Yang, Y.H. Yue, Z. Gao, Y. Tang, Chem. Mater. 17 (2005) 2582–2587.
[49] D.G. Shchukin, D.V. Sviridov, J. Photochem. Photobiol. C 7 (2006) 23–39.
[50] H. Weiß, A. Fernández, H. Kisch, Angew. Chem. Int. Ed. 40 (2001) 3825–3827.
[51] H. Kisch, H. Weiß, Adv. Funct. Mater. 12 (2002) 483–488.
[52] G. Herzberg, Molecular Spectra and Molecular Structure. II. Infrared and Raman Spectra of Polyatomic Molecules, van Nostrand Reinhold Co., New York, 1966, p. 1.
[53] S. Zhou, A.K. Ray, Ind. Eng. Chem. Res. 42 (2003) 6020–6033.
[54] A. Henglein, Top. Curr. Chem. 143 (1988) 113–180.
[55] T. Vossmeyer, L. Katsikas, M. Giersig, I.G. Popović, K. Diesner, A. Chemseddine, A. Eychmüller, H. Weller, J. Phys. Chem. 98 (1994) 7665–7673.
[56] J. Nanda, B.A. Kuruvilla, D.D. Sarma, Phys. Rev. B 59 (1999) 7473–7479.
[57] A. Henglein, Ber. Bunsenges. Phys. Chem. 86 (1982) 301–305.
[58] A. Henglein, et al., Chem. Phys. Lett. 132 (1986) 133–136.
[59] B. Tell, T.C. Damen, S.P.S. Porto, Phys. Rev. 144 (1966) 771–774.